Polar nature of domain boundaries in purely ferroelastic $Pb_3(PO_4)_2$ investigated by second harmonic generation microscopy

H. Yokota,[1,*] S. Matsumoto,[2] E. K. H. Salje,[3] and Y. Uesu[4]

[1]*Department of Physics, Chiba University, 1-33 Yayoi-cho, Inage-ku, Chiba-shi, Chiba 263-8522, Japan*
[2]*Department of Physics, Faculty of Science and Engineering, Chiba University, 1-33 Yayoi-cho, Inage-ku, Chiba-shi, Chiba 263-8522, Japan*
[3]*Department of Earth Sciences, Cambridge University, Downing Street, Cambridge CB2 3EQ, United Kingdom*
[4]*Department of Physics, Faculty of Science and Engineering, Waseda University, 3-4-1 Okubo, Shinjuku-ku, Tokyo 169-8555, Japan*

(Received 26 April 2019; published 1 July 2019)

Domain boundaries in lead phosphate, $Pb_3(PO_4)_2$, are investigated by using second harmonic generation (SHG) microscopy. It is revealed that they are polar while the bulk is a purely ferroelastic, centrosymmetric material. $Pb_3(PO_4)_2$ contains W and W' walls with different orientations. The SHG microscopy shows that both W and W' walls are polar, in striking contrast to the bulk, where the macroscopic polarity is forbidden by symmetry. The strongest polarity is observed in the W walls with a local symmetry of monoclinic m. The W' walls are also monoclinic but with symmetry 2. This material is hence a new candidate for domain-boundary-induced ferroelectricity while the bulk remains fully inactive. An application of small stress to a W wall easily changes the boundary configuration without changing the type of domain boundary; i.e., the W-wall nature is conserved. While $Pb_3(PO_4)_2$ was so far suggested as a device material for acousto-optic switchers, the present study adds the possibility that light scattering can be modified also by electric fields.

DOI: 10.1103/PhysRevB.100.024101

I. INTRODUCTION

Domains are a fundamentally important concept for all ferroic materials because they represent energetically equivalent states of the order parameter. These states can, in most cases, be switched among each other by external forces and therefore define key ferroic characteristics, such as the hysteresis in ferromagnets, ferroelectrics, and ferroelastics. Structural configurations, and their changes under an external field and with temperature, have been intensively studied and have become well understood for many ferroics since the first discovery of the Barkhausen effect ca. 100 years ago [1]. In contrast, domain boundaries (DBs) that separate domains with different orientational states have traditionally been treated as a mere concomitant phenomenon of multidomain states. Particularly in ferroelectric or ferroelastic crystals DBs are atomically thin [2–6], in contrast to Bloch- or Néel-type walls of ferromagnets. Observation of any structural or physical property of DBs was previously difficult because the number of atoms in DBs is typically less than 1 ppm of the total crystal. Over the past decade, DBs in ferroics have been found to clearly exhibit unique functional properties different from those in the bulk [2]. High conductivity [7–12], superconductivity [7], photovoltaic effect [13], and the polar nature in a nonpolar bulk [14–20] are examples. DBs have hence attracted attention for use in next-generation nanotechnology devices due to their small size and controllability of switchable state parameters via chemical doping. Among ferroics, ferroelastic DBs have the additional advantage of existing in high-density states, which is suitable for large-capacity memory devices [21–23]. In this case, the position of a DB can be moved by applying extremely small stresses to position the wall at a suitable location in a monolithic device component.

The first material for which polarity was found at DBs is $CaTiO_3$ (CTO). Polarity was theoretically predicted [24,25] and experimentally observed using an aberration-corrected transmission electron microscope (TEM) [15]. The Ti atom displaces inside the DBs of CTO, which creates a relatively large polarization. The polar nature at DBs has also been reported in other ferroelastic materials, such as $SrTiO_3$, and $LaAlO_3$, using resonance piezoelectric spectroscopy (RPS) [14,16,19], a piezoelectric force microscope (PFM) [19], and a second harmonic generation microscope (SHGM) [18,20,26]. Based on these results, a more general question that is interesting to ask is whether most DBs in pure ferroelastic materials exhibit a polar nature, as theoretically predicted [27–29]. None of the previously investigated $CaTiO_3$ and $LaAlO_3$ contains known ferroelectric ground states in their phase diagram, and boundary polarity is a specific phenomenon of the DBs. In this context, determining the type of polarization configuration of complex DBs, such as Ising, Bloch, or Néel walls [30,31], in ferroelastics, for which polarity has not yet been observed, is also important to widen the scope of possible materials for DB applications.

In the present study, we chose the archetypal ferroelastic lead phosphate, $Pb_3(PO_4)_2$, which is known to be ferroelastic without any ferroelectric instability. $Pb_3(PO_4)_2$ was the first ferroelastic material [32] for which a full ferroelastic hysteresis loop was obtained [33,34]. $Pb_3(PO_4)_2$ exhibits an improper ferroelastic phase transition at 453.7 K from trigonal $R\bar{3}m$ to monoclinic $C2/c$, which is associated with a condensation of the L points on the Brillouin zone boundary [35]. The phase transition has been described by a three-state Potts

*Corresponding author: hiroko.9bq@chiba-u.jp

model [36]. The ferroelastic phase is characterized by the displacement of Pb ions perpendicular to the triad axis and tilting of the PO_4 tetrahedra [4,37]. Additional symmetry breaking has been proposed in the paraelastic phase due to the existence of monoclinic microstructures. Concerning the ferroelastic phase, the possibility of monoclinic $C2$, which is noncentrosymmetric, has been reported based on neutron diffraction and SHGM [38].

Lead phosphate and its isostructural vanadium compounds were proposed for use in acousto-optic devices for switching of laser beams in 1976 [39]. While this development was not pursued in industry, it initiated much research into the growth and applications of these materials [40–43]. Bleser *et al.* found second harmonic (SH) activity near the sample surface and argued that this activity may not be related to intrinsic symmetry breaking [42]. Furthermore, an RPS experiment found no evidence of a piezoelectric nature in the ferroelastic phase [44], which supports that the space group of the low-temperature phase is monoclinic $C2/c$, which possesses centrosymmetry. We use SHG to examine the polar nature at DBs in $Pb_3(PO_4)_2$. SHG relating to electric-dipole interactions only occurs in materials that do not possess centrosymmetry and is a very sensitive probe of local symmetry breaking. Because the SHG process relates to third-rank polar tensor components, i.e., the nonlinear optical susceptibility tensor d, the polarization dependence of the SH intensity directly reflects the point-group symmetry. Determination of the point group is essential to clarify the polar nature because only 10 point groups belong to polar classes among 20 point groups that exhibit piezoelectricity and SHG. Another important aspect that we can obtain from the polarimetry analysis of SH intensity is the dielectric polarization orientation. In many point groups, the polarization direction is parallel to the principle axis. Therefore, the determination of the point group and crystallographic axes makes it possible to uniquely determine the polarization orientation. See Ref. [45] for the precise description of the analyses.

II. EXPERIMENT

$Pb_3(PO_4)_2$ single crystals are grown by the Czochralski method [46,47]. A $Pb_3(PO_4)_2$ sample with a thickness of 160 μm is used as a specimen. It has a cleavage plane with a (0001) hexagonal axis. The DB structure is examined using a polarization microscope under a crossed Nicol configuration. We select three regions that contain DBs with different orientations and perform SHG microscope observations. We use an Nd:YVO_4 laser with a wavelength of 1064 nm, a repetition frequency of 40 kHz, a laser power of 0.125 W, and a laser energy of 3.125 μJ as a fundamental wave. The laser power is adjusted by an attenuator composed of a half-wave plate and a thin-film polarizer. To monitor the laser stability, we measure the intensity of the fundamental wave using a photodetector during the experiment and the obtained SH signal is normalized by the square of the fundamental wave intensity. A fundamental wave is focused on the sample by an objective lens with a numerical aperture of 0.7. The SH wave generated from the sample is collected by an objective lens with the same numerical aperture. After passing through a spectrometer, the SH waves are detected by a photomultiplier tube synchronized with the fundamental wave by a lock-in amplifier. To construct three-dimensional (3D) SHG images, we adopt a scanning system equipped with a piezoactuator stage for the lateral directions (XY plane) and a stepping motor for the depth direction (Z axis). The typical scanning steps used in the experiments are 0.2 μm for the lateral directions and 4 μm for the depth direction. This system enables us to obtain 3D images without any destruction or special treatment of the sample. We use a half-wave plate and an analyzer to change the polarization directions of the fundamental wave and SH wave, respectively.

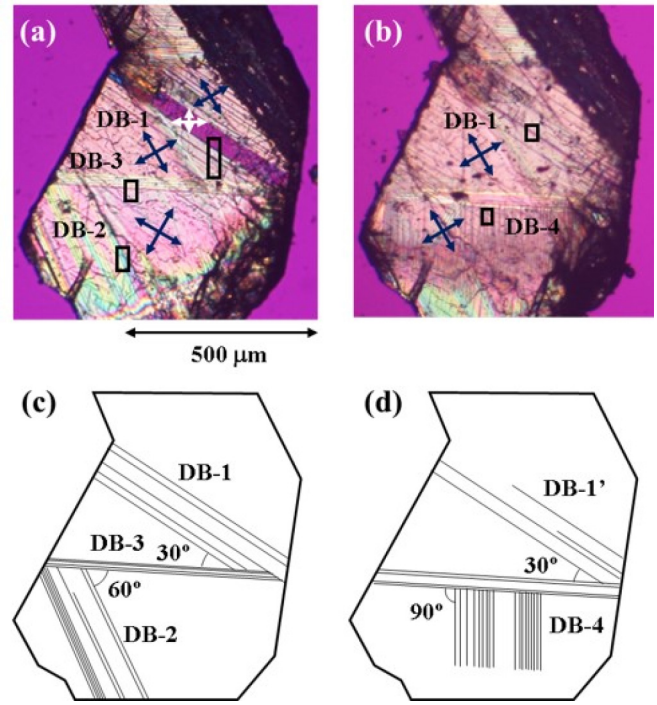

FIG. 1. Polarization microscope images under a crossed Nicol configuration (a) before the application of stress and (b) after the application of stress. A compressive stress is applied along a direction almost perpendicular to DB-1. Blue and white arrows correspond to the extinction positions for each area. No extinction position is found for the area containing DB-3. In (b), a new DB, DB-4, appears after applying stress; (c) and (d) are schematic images of (a) and (b), respectively.

III. RESULTS AND DISCUSSIONS

Figure 1(a) shows a polarization microscope image under a crossed Nicol configuration. This image exhibits a stripe domain pattern commonly observed in $Pb_3(PO_4)_2$ [47–50] and three types of DBs with different orientations are observed (hereafter called DB-1, DB-2, and DB-3, and the corresponding areas of D1, D2, and D3). It is known that nonstoichiometries in $Pb_3(PO_4)_2$ typically lead to zigzag-shaped DB configurations [51]. Since there is no zigzag pattern in our specimen, we conclude that $Pb_3(PO_4)_2$, which we use in our experiments, is nearly stoichiometric. DB-1 is inclined 30° from DB-3, and the angle between DB-2 and DB-3 is 60°. Although D3 shows no extinction position, the other two regions clearly exhibit extinction positions. The extinction

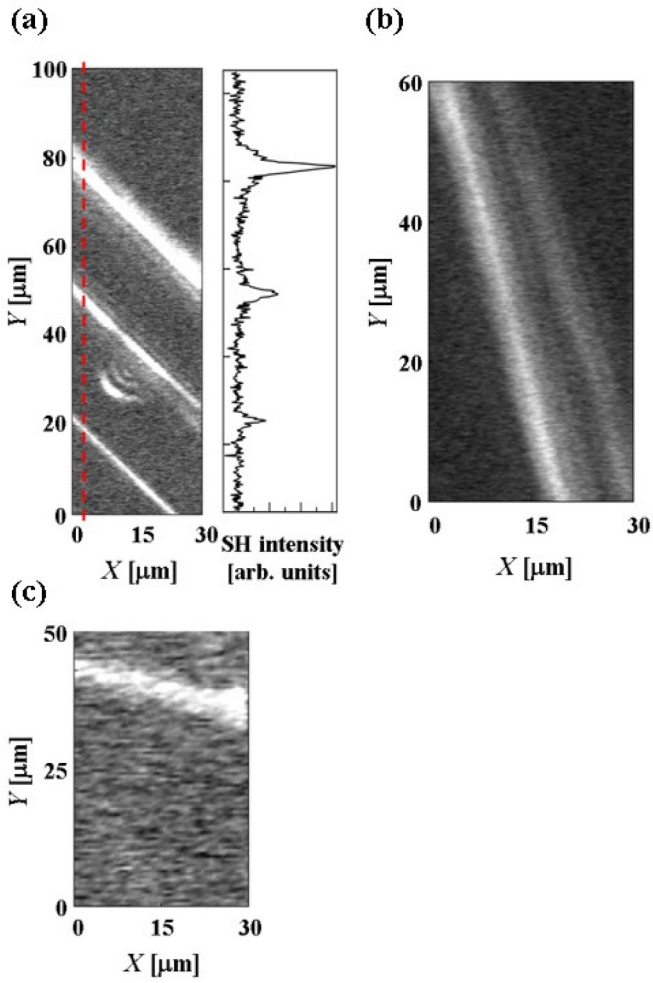

FIG. 2. 2D images of the distributions of SH waves from the areas with (a) DB-1, (b) DB-2, and (c) DB-3. SH images were taken from the enclosed areas shown in Fig. 1(a). The bright region corresponds to the area where SH waves are generated. The 1D plot for DB-1 along the red dashed line is included on the right of (a). A high SN ratio confirms that DBs are SH active, contrary to the fact that no SH intensity is observed in the domain itself.

positions of D1 are inclined by 30° and 60° from DB-1, and the inclination angle from DB-2 in D2 is 30° (shown in Fig. 1 as white or blue arrows). Since the crystal structure of $Pb_3(PO_4)_2$ is monoclinic $C2/c$, it has a biaxial crystal symmetry, and one of the optical principal axes is parallel to the crystallographic x_2 axis. Because the cleavage plane is perpendicular to the triad axis of the trigonal setting, the monoclinic x_2 axis lies in the cleavage plane, and this direction appears as the extinction position under a crossed Nicol configuration. Therefore, the orientation of the monoclinic x_2 axis was determined from the polarization microscope observations.

Figures 2(a), 2(b), and 2(c) show two-dimensional (2D) images of the distributions of SH waves from the areas that contain DB-1, DB-2, and DB-3, respectively. It is well known that a surface often produces a strong SH intensity because of the symmetry lowering and surface piezoelectricity [52,53]. To avoid this surface effect, we perform a one-dimensional

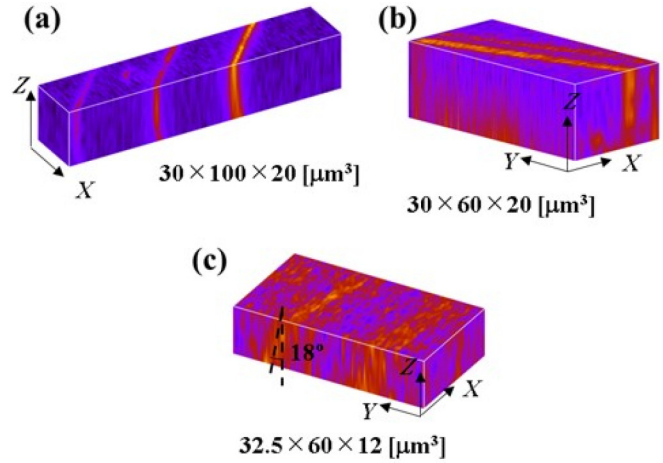

FIG. 3. Constructed 3D images of the SH intensity from (a) DB-1, (b) DB-2, and (c) DB-3. A bright color corresponds to the region where strong SH intensity is detected. SH intensity does not change along the depth direction. DB-1 and DB-2 are almost perpendicular to the sample surface. In contrast, DB-3 is inclined around 18° from the sample surface.

(1D) scan along the Z axis using a 532-nm reference wave and the focal position is adjusted to the middle of the specimen to obtain these images. SH-active regions are observed as bright lines, as shown in Fig. 2. The SHG distributions are homogeneous along each SH-active line. The observed SH activities do not originate from the domain itself since $Pb_3(PO_4)_2$ is a purely ferroelastic material with centrosymmetry. Based on a comparison with the polarization microscope image, we can conclude that the SH-active lines equate with DBs. Although the SH intensity is relatively weak compared with normal nonlinear optical materials ($\sim 10^{-8}$ times weaker than the d_{31} component of $LiNbO_3$), the signal-to-noise (SN) ratio is extremely high, i.e., 60:1 in the case of DB-1. Such a high SN ratio confirms the validity of our experimental results. Among the three DBs, the SH intensity from DB-3 is rather weak compared with the others. Additionally, the SH-active line is wider than those for the other two DBs. We explain the origin of this phenomenon later. Kiat *et al.* observed SH signals from bulk $Pb_3(PO_4)_2$ and claimed that the intensity is approximately 10^{-2} times smaller than that of the d_{36} component of KH_2PO_4 [38]. We do not detect any SH intensities from domains, and the SH intensity that we observe from the DBs is much weaker than the intensity these authors observed. Thus, the SH signals that we observe here are intrinsically different. Bleser *et al.* reported the observation of SH intensity from $Pb_3(PO_4)_2$ [42] and explained it as a surface effect, which is possibly related to structural imperfections. Therefore, we measure the SH intensities as a function of the fundamental laser power and confirm that the SH intensity is proportional to the power of the fundamental laser intensity. This result suggests that the SH signal we obtain is an intrinsic effect of the DBs.

Several 2D scans are carried out with different depths to construct 3D perspective images of the distributions of the SH waves from the DBs. Figures 3(a)–3(c) exhibit 3D images for the different DBs. The magnitude of the SH intensity does

not change as a function of depth, which indicates that the DBs are SH active inside the specimen. For DB-1 and DB-2, the DBs are almost perpendicular to the sample surface. In the case of DB-3, the DB is inclined approximately 18° from the surface.

For ferroelastics, the orientations of DBs between two adjacent domains are theoretically determined based on strain compatibility theory. Two types of DBs exist: one corresponds to crystallographically prominent planes of fixed indices, known as the W wall, and the other is the W' wall [50]. The orientation of a W' wall is determined by the relative magnitude of the components of the second-rank tensor representing the spontaneous strain. Thus, the orientation of a W' wall depends on the temperature and other external stimuli. $Pb_3(PO_4)_2$ exhibits a first-order ferroelastic phase transition at 453.6 K from trigonal $R\bar{3}m$ to monoclinic $C2/c$, which belongs to $\bar{3}mF2/m$ species according to the Aizu notation [54]. The orientations of DBs in this class can be expressed by the following equations:

$$y = 0, \tag{1}$$

$$y = \sqrt{3}x, \tag{2}$$

$$y = -\sqrt{3}x, \tag{3}$$

$$z = -ax/c, \tag{4}$$

$$a(\sqrt{3}y + x) - 2cz = 0, \tag{5}$$

$$a(\sqrt{3}y - x) + 2cz = 0. \tag{6}$$

Here, x, y, and z are the orthogonal coordinate system of the prototypic phase, in which the triad axis of the trigonal phase is along the z axis, and the monoclinic x_2 axis is parallel to y; a and c are the strain tensor components describing

$$\begin{pmatrix} -a & 0 & c \\ 0 & a & 0 \\ c & 0 & 0 \end{pmatrix}. \tag{7}$$

The magnitudes of a and c are obtained from the lattice parameters of the monoclinic structure, and the relationships between these tensor components and the monoclinic lattice parameters (x_1, x_2, x_3, and β) are expressed as

$$a = \frac{x_2 - x_3/\sqrt{3}}{2x_2}, \tag{8}$$

$$c = \frac{x_3 + 3x_1 \cos\beta}{6x_1 \sin\beta}. \tag{9}$$

The values of a and c at room temperature are $a = 20.55 \times 10^{-3}$ and $c = 6.72 \times 10^{-3}$, respectively [50]. Among the six types of DBs, the DBs expressed by Eqs. (1)–(3) belong to W walls since the orientations of these boundaries are uniquely determined by the symmetry operations and do not depend on the numerical values of the strain tensor components. Taking into account the crystallographic relationships between the cleavage plane and the DBs expressed by Eqs. (1)–(6), the inclination angles of DBs from the cleavage plane can be calculated. Substituting a and c values into Eqs. (4)–(6), the tilt angle of W' walls from the cleavage plane can be calculated. The angle between all W' walls and the cleavage plane is 18.10°, while W walls are perpendicular to the cleavage plane. In addition, the angle between W walls and the monoclinic x_2 axis is either 30° or 90°. Based on the polarization microscope observations and 3D observations of the SH distributions, we can identify DB-3 as a W' wall and DB-1 and DB-2 as W walls. The inclination angle of DB-3 coincides well with the predicted value. Moreover, the fact that only a few DBs are assigned as DB-3 supports our conclusion since the W' wall is a minor DB in $Pb_3(PO_4)_2$ [47]. Since a W' wall is inclined from the surface, a lack of a clear extinction position is not surprising. Furthermore, the width of the SH-active line could be wider than that of the W walls because it is a superposition of images along the Z direction over 4 μm.

To determine the symmetry of the DBs, the polarization dependencies of the SH intensities are measured. The polarization directions of a fundamental wave and an SH wave are fixed as parallel to each other and rotate together every 6° or 12°. The 2D images thus obtained are divided into several hundred small grids to take an average, and polar diagrams describing the anisotropy of the SHG are finally constructed [55]. Figures 4(a) and 4(b) show the 2D polar diagrams of DB-1 and DB-2, respectively. The polarization dependencies for each DB are collected in the same regions as for Fig. 2. Apart from the DBs, the SH intensity is null in any polarization direction. Although the shape of the SH anisotropy is similar for the same type of DB, the angles of the SH maxima are slightly different for DB-1, similar to ferroelastic $CaTiO_3$ [18]. This difference is possibly caused by the interaction from the neighboring DBs reducing the electrostatic energy by changing the polarization direction. In Figs. 4(c), 4(d), and 4(e), expanded plots of the polarization dependences for DB-1, DB-2, and DB-3, respectively, are shown. For comparison, the polar diagram from the domain itself is plotted in Fig. 4(f). We attempt to fit the experimental data with the point groups that are subgroups of $R\bar{3}m$. Moreover, all W walls are mirror planes, and W' walls contain a twofold axis based on strain compatibility theory [56,57]. Based on these criteria, we choose monoclinic m for the W wall and monoclinic 2 for the W' wall to analyze the polarization dependence of the SH intensity. In the case of symmetry m, SH maxima should be either parallel or perpendicular to the DBs. However, in our results, the SH maxima angles for W walls are approximately 50° from the predicted orientation. This deviation is probably due to the strain effect from the neighboring DBs. To probe this hypothesis, we conduct SHG measurements on a 5% Ca-doped $Pb_3(PO_4)_2$ sample with fewer DBs. Figure 5(a) shows the image taken by a polarization microscope with a crossed Nicol configuration. Only three DBs are observed in this region, and the separations between neighboring DBs are much wider than those in the pure sample, which means that each DB feels less strain in Ca-doped $Pb_3(PO_4)_2$. In Fig. 5(b), a 2D image of the SH wave distributions is demonstrated, which suggests that only DBs are SH active. A constructed 3D image of the SH wave distribution is shown in Fig. 5(c). The DBs retain their SH activities inside the specimen with almost the same intensities. Since both DBs are perpendicular to the cleavage plane, these DBs belong to W walls. The polarization dependence of the SH intensity from one of these

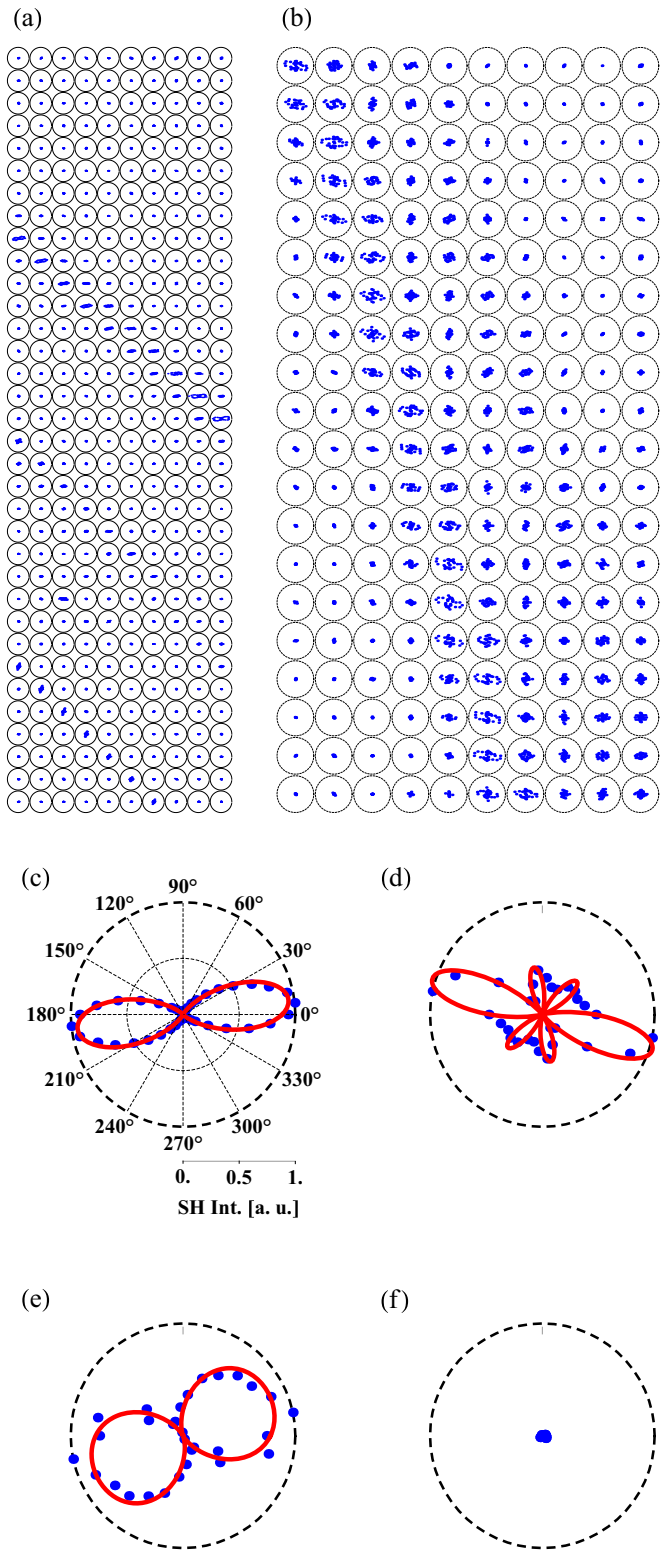

FIG. 4. Polar diagram mappings of (a) DB-1 and (b) DB-2. Expanded polarization dependencies of the SH intensity are shown for (c) DB-1, (d) DB-2, and (e) DB-3. Blue dots correspond to the experimental data and red lines correspond to the fitting results. DB-1 and DB-2 are fitted with monoclinic m and monoclinic 2 is assumed for DB-3. (f) The polarization dependence for the domains is shown for comparison. This dependence is almost zero for all directions.

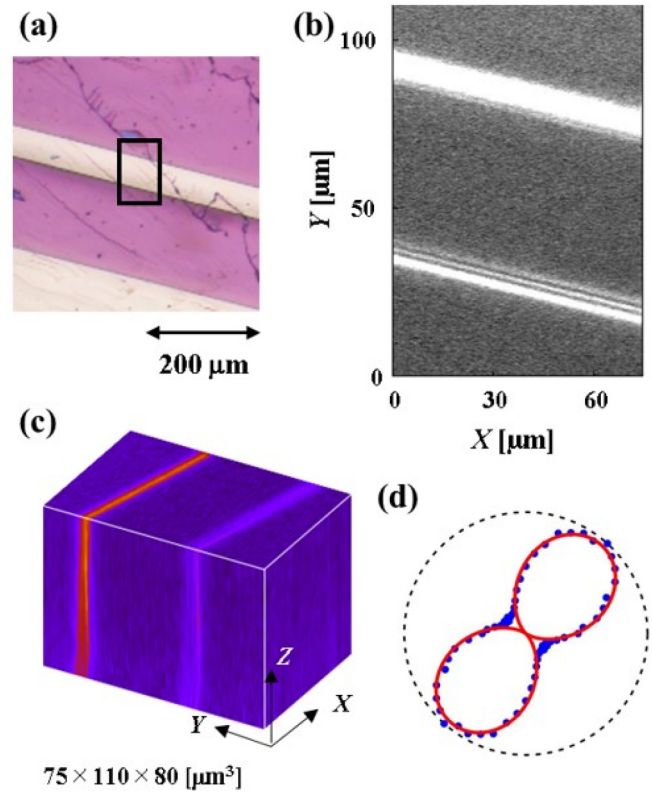

FIG. 5. (a) Polarization microscope image under a crossed Nicol configuration, (b) 2D image of the SH wave distribution, (c) 3D image of the SH intensity, and (d) polarization dependence of the SH intensity for 5% Ca-doped $Pb_3(PO_4)_2$. There is only one type of DB in this sample and this DB is SH active.

DBs is summarized in Fig. 5(d). Although the shape of the anisotropy is similar to that for DB-1, the direction of the SH maximum is different and almost perpendicular to the DB in the case of Ca-doped $Pb_3(PO_4)_2$. This result indicates that the strain induced by neighboring DBs affects the properties of the DB. Due to the high density of DBs in pure $Pb_3(PO_4)_2$, the orientations of the SH maxima are influenced by a strain and are oriented away from the symmetry-permitted directions. Further systematic experiments are needed to confirm the DB density effect using a pure $Pb_3(PO_4)_2$.

SHG is a nonlinear optical process, and a nonlinear polarization P related to the SHG process can be expressed as

$$P_i = \sum_{j,k} d_{ijk} E_j E_k. \tag{10}$$

Here E is the electric field of a fundamental wave and i, j, and k represent the polarization direction of the relevant fields. In the case of m, the monoclinic x_2 axis is perpendicular to the mirror plane. Therefore, the direction of the monoclinic x_2 axis is determined to be normal to the DBs. The nonlinear optical susceptibility tensor d of m is given by

$$\begin{pmatrix} d_{11} & d_{12} & d_{13} & 0 & d_{15} & 0 \\ 0 & 0 & 0 & d_{24} & 0 & d_{26} \\ d_{31} & d_{32} & d_{33} & 0 & d_{35} & 0 \end{pmatrix}, \tag{11}$$

where the subscripts of d represent the directions of the axes referring to the Cartesian coordinate system, and the monoclinic x_2 axis is parallel to the axis labeled 2. The Voigt notation is used to describe the tensor components. To apply Eq. (11) to our experimental results, we also need to determine axes 1 and 3. In the case of a monoclinic structure, there is no symmetry restriction about these two axes, and we cannot uniquely determine their orientations. For generalization, we assume that neither of the axes lies in the XY plane and they need to rotate anticlockwise through an angle ϕ about the axis 2. This process makes axis 1 to be on the XY plane. The rotation matrix R is expressed as

$$R(\phi) = \begin{pmatrix} \cos\phi & 0 & -\sin\phi \\ 0 & 1 & 0 \\ \sin\phi & 0 & \cos\phi \end{pmatrix}. \tag{12}$$

By application of the rotation matrix, we have

$$d'_{ijk} = R_{il}R_{jm}R_{kn}d_{lmn} \tag{13}$$

as a transformed nonlinear optical susceptibility tensor d'. The transformed d' matrix has the same independent tensor components as the d tensor. Therefore, we can simply apply Eq. (11) to describe the anisotropy of the SH intensity. We fit the experimental data with the following equations:

$$I^{(2\omega)} \propto P^2 = (P_1\cos\theta + P_2\sin\theta)^2, \tag{14}$$

$$\begin{aligned} P_1 &\propto d'_{11}{E_1}^2 + d'_{12}{E_2}^2, \\ P_2 &\propto d'_{26}E_1E_2, \end{aligned} \tag{15}$$

$$\begin{aligned} E_1 &= E_0\cos\theta, \\ E_2 &= E_0\sin\theta. \end{aligned} \tag{16}$$

In the above equations, θ is the rotation angle of the coupled polarizer and analyzer from axis 1. The results are shown in Figs. 4(c) and 4(d) as red solid lines. This model reproduces the experimental data well, and we can conclude that the point group of the W wall is monoclinic m.

For the W' wall, the fitting of the polarization dependence of the SH intensity follows a similar procedure as that for the W wall. In the case of the W' wall, we use

$$I^{(2\omega)} \propto P^2 = \{(d'_{16} + d'_{21})\cos^2\theta\sin\theta + d'_{22}\sin^3\theta\}^2. \tag{17}$$

Here, the same geometry is applied as with the W wall, and d' is the transformed nonlinear optical susceptibility tensor of monoclinic 2. The obtained fitting result is shown in Fig. 4(e) as a red line. We apply several different models, and the best fitting results are obtained with monoclinic m for the W wall and monoclinic 2 for the W' wall. We also apply the same analysis to Ca-doped $Pb_3(PO_4)_2$ and the SH anisotropy can be well explained by monoclinic symmetry m. These results are consistent with strain compatibility theory, and our results suggest that all ferroelastic DBs observed in $Pb_3(PO_4)_2$-based materials are polar.

The final goal of DB engineering [2] is to apply the exotic physical properties observed at DBs to devices. To realize DB devices, the DB positions and properties must be controlled by an external stimulus. In the case of $CaTiO_3$, we succeeded in creating functional DBs by applying a compressive stress [20]. However, the magnitude of the stress was too high to apply in future devices. In contrast to $CaTiO_3$, $Pb_3(PO_4)_2$ is known to be a soft ferroelastic and a relatively small stress can change the DB structure. We apply a compressive stress from a direction almost perpendicular to DB-1 by using a pair of tweezers. Figure 1(b) shows a polarization microscope image of $Pb_3(PO_4)_2$ after the application of stress. A small stress drastically changes the DB structure, and this DB structure remains after releasing the stress. DB-2 almost disappears, and new DBs (DB-4), perpendicular to DB-3, appear below DB-3. The extinction position of D4 is the same as that of D1 and is inclined by 60° from DB-3 [shown as the blue arrows in Fig. 1(b)]. Figures 6(a) and 6(b) show SH images of the areas with DB-1 and DB-4, respectively. After the application of stress, DB-1 is still SH active, and its intensity does not change. Additionally, the newly appeared DB-4 is also SH active. 3D images for DB-1 and DB-4 are shown in Figs. 7(a) and 7(b). Both DBs remain SH active inside the sample and are almost perpendicular to the cleavage plane. This result suggests that DB-4 belongs to the W wall and that the W wall

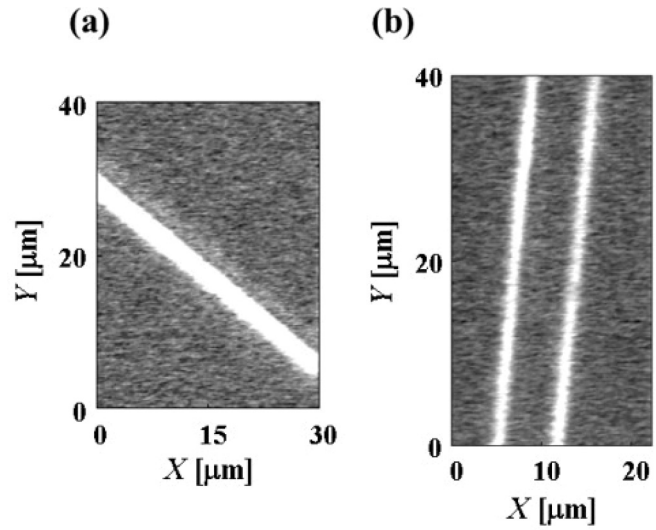

FIG. 6. 2D images of SH wave distributions from (a) DB-1 and (b) DB-4 after the application of stress. These images were obtained from the enclosed area shown in Fig. 1(b). After the application of stress, DB-1 is still SH active and the newly appeared DB-4 is also SH active.

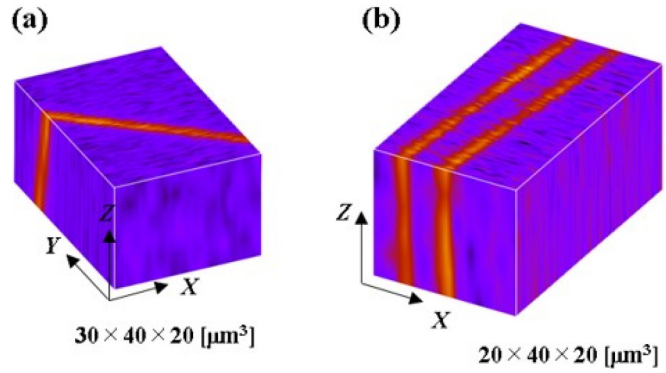

FIG. 7. Constructed 3D SH images of (a) DB-1 and (b) DB-4. SH activity remains inside the sample for both cases. SH-active planes are almost perpendicular to the cleavage plane.

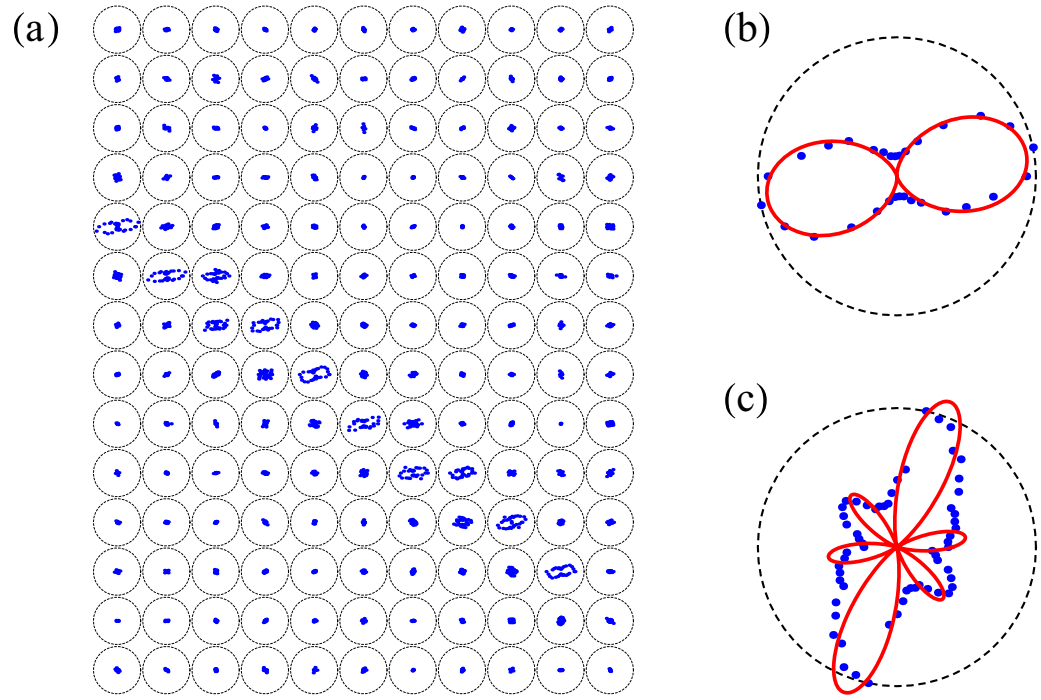

FIG. 8. (a) Polar diagram mapping of DB-1 after the application of stress. Expanded polarization dependencies of the SH intensity are shown for (b) DB-1 and (c) DB-4. Both experimental data sets are fitted according to monoclinic *m,* shown as red lines.

is preferred DB under stress. Polar diagrams of DB-1 and polarization dependencies of the SH intensities from DB-1 and DB-4 are shown in Figs. 8(a)–8(c). In the case of DB-1, the SH anisotropy does not change, and its behavior can be explained by monoclinic symmetry *m*. For DB-4, we also fit the experimental data with monoclinic *m*. The fitting result is not as good as that for DB-1 since the DB structure near DB-4 is more complex than that near DB-1 and the existence of DB-3 affects the polarization dependence.

IV. CONCLUSION

In this work, we perform SHG microscope observations on improper ferroelastic $Pb_3(PO_4)_2$. We confirm that all DBs of $Pb_3(PO_4)_2$ with different types and orientations are polar. Therefore, the polar nature at the domain boundary is not limited to their characters. Additionally, the polar nature at the DB has been also reported in other ferroelastics, e.g., $CaTiO_3$, $LaAlO_3$, and $SrTiO_3$, whose crystal structures belong to different space groups. This fact leads us to a confirmation that the polar nature of DBs of ferroelastics does not depend on the certain parent phases and it could be ubiquitous phenomena in ferroelastics. The polar nature at the DBs in ferroelastics can be interpreted by the symmetry lowering and the symmetries are determined from the anisotropy of the SH intensity. The polarity orientation is strongly influenced by the neighboring DBs through the strain effect. We also show that an application of a small compressive stress can change the DB structure while maintaining its functionality. This result suggests the possibility of controlling DBs for further applications such as in acousto-optic switches and ferrielectric switching related to the Pb positions in oxygen tetrahedras.

ACKNOWLEDGMENTS

H.Y. is grateful to the Ministry of Education, Culture, Sports, Science and Technology in Japan for financial support (Grant No. 17K05489) and the Iketani Science and Technology Foundation (Grant No. 0311045-A). E.K.H.S. is grateful to EPSRC for financial support (Grant No. EP/P024904/1).

[1] H. Barkhausen, Phys. Z. **20**, 401 (1919).
[2] E. K. H. Salje, ChemPhysChem **11**, 940 (2010).
[3] P. Marton, I. Rychetsky, and J. Hlinka, Phys. Rev. B **81**, 144125 (2010).
[4] E. K. H. Salje, Annu. Rev. Mater. Res. **42**, 265 (2012).
[5] J. Hlinka, J. Privratska, P. Ondrejkovic, and V. Janovec, Phys. Rev. Lett. **116**, 177602 (2016).
[6] R. Ayroles, J. Torres, J. Aubree, C. Roucau, and M. Tanaka, Appl. Phys. Lett. **34**, 4 (1979).
[7] A. Aird and E. K. H. Salje, J. Phys. Condens. Matter **10**, L377 (1998).
[8] J. Seidel, L. W. Martin, Q. He, Q. Zhan, Y.-H. Chu, A. Rother, M. E. Hawkridge, P. Maksymovych, P. Yu, M. Gajek, N. Balke, S. V. Kalinin, S. Gemming, F. Wang, G. Catalan, J. F. Scott, N. A. Spaldin, J. Orenstein, and R. Ramesh, Nat. Mater. **8**, 229 (2009).
[9] J. Seidel, P. Maksymovych, Y. Batra, A. Katan, S.-Y. Yang, Q. He, A. P. Baddorf, S. V. Kalinin, C.-H. Yang, J.-C. Yang,

Y.-H. Chu, E. K. H. Salje, H. Wormeester, M. Salmeron, and R. Ramesh, Phys. Rev. Lett. **105**, 197603 (2010).
[10] Y. Kim, M. Alexe, and E. K. H. Salje, Appl. Phys. Lett. **96**, 032904 (2010).
[11] P. Maksymovych, J. Seidel, Y. H. Chu, P. Wu, A. P. Baddorf, L.-Q. Chen, S. V. Kalinin, and R. Ramesh, Nano Lett. **11**, 1906 (2011).
[12] S. Farokhipoor and B. Noheda, Phys. Rev. Lett. **107**, 127601 (2011).
[13] S. Y. Yang, J. Seidel, S. J. Byrnes, P. Shafer, C.-H. Yang, M. D. Rossell, P. Yu, Y.-H. Chu, J. F. Scott, J. W. Ager, L. W. Martin, and R. Ramesh, Nat. Nanotechnol. **5**, 143 (2010).
[14] P. Zubko, G. Catalan, A. Buckley, P. R. L. Welche, and J. F. Scott, Phys. Rev. Lett. **99**, 167601 (2007).
[15] S. Van Aert, S. Turner, R. Delville, D. Schryvers, G. Van Tendeloo, and E. K. H. Salje, Adv. Mater. **24**, 523 (2012).
[16] J. F. Scott, E. K. H. Salje, and M. A. Carpenter, Phys. Rev. Lett. **109**, 187601 (2012).
[17] E. K. H. Salje, O. Aktas, M. A. Carpenter, V. V. Laguta, and J. F. Scott, Phys. Rev. Lett. **111**, 247603 (2013).
[18] H. Yokota, H. Usami, R. Haumont, P. Hicher, J. Kaneshiro, E. K. H. Salje, and Y. Uesu, Phys. Rev. B **89**, 144109 (2014).
[19] E. K. H. Salje, M. Alexe, S. Kustov, M. C. Weber, J. Schiemer, G. F. Nataf, and J. Kreisel, Sci. Rep. **6**, 27193 (2016).
[20] H. Yokota, S. Niki, R. Haumont, P. Hicher, and Y. Uesu, AIP Adv. **7**, 085315 (2017).
[21] X. Ding, Z. Zhao, T. Lookman, A. Saxena, and E. K. H. Salje, Adv. Mater. **24**, 5385 (2012).
[22] E. K. H. Salje, X. Ding, Z. Zhao, and T. Lookman, Appl. Phys. Lett. **100**, 222905 (2012).
[23] D. D. Viehland and E. K. H. Salje, Adv. Phys. **63**, 267 (2014).
[24] B. Houchmandzadeh, J. Lajzerowicz, and E. Salje, J. Phys. Condens. Matter **3**, 5163 (1991).
[25] L. Goncalves-Ferreira, S. A. T. Redfern, E. Artacho, and E. K. H. Salje, Phys. Rev. Lett. **101**, 097602 (2008).
[26] H. Yokota, S. Matsumoto, E. K. H. Salje, and Y. Uesu, Phys. Rev. B **98**, 104105 (2018).
[27] A. N. Morozovska, E. A. Eliseev, M. D. Glinchuk, L.-Q. Chen, and V. Gopalan, Phys. Rev. B **85**, 094107 (2012).
[28] P. Zubko, G. Catalan, and A. K. Tagantsev, Annu. Rev. Mater. Res. **43**, 387 (2013).
[29] E. K. H. Salje, S. Li, M. Stengel, P. Gumbsch, and X. Ding, Phys. Rev. B **94**, 024114 (2016).
[30] S. Cherifi-Hertel, H. Bulou, R. Hertel, G. Taupier, K. D. Dorkenoo, C. Andreas, J. Guyonnet, I. Gaponenko, K. Gallo, and P. Paruch, Nat. Commun. **8**, 15768 (2017).
[31] G. De Luca, M. D. Rossell, J. Schaab, N. Viart, M. Fiebig, and M. Trassin, Adv. Mater. **29**, 1605145 (2017).
[32] L. H. Brixner, P. E. Bierstedt, W. F. Jaep, and J. R. Barkley, Mater. Res. Bull. **8**, 497 (1973).
[33] E. Salje and G. Hoppmann, Mater. Res. Bull. **11**, 1545 (1976).
[34] E. K. H. Salje, *Phase Transitions in Ferroelastic and Co-Elastic Crystals* (Cambridge University Press, Cambridge, UK, 1991).
[35] J. Torres, Phys. Status Solidi **71**, 141 (1975).
[36] E. Salje and V. Devarajan, J. Phys. C Solid State Phys. **14**, L1029 (1981).
[37] U. Keppler, Z. Kristallogr. **132**, 228 (1970).
[38] J. M. Kiat, Y. Yamada, G. Chevrier, Y. Uesu, P. Boutrouille, and G. Calvarin, J. Phys. Condens. Matter **4**, 4915 (1992).
[39] E. Salje, Phys. Status Solidi **33**, K165 (1976).
[40] E. Dudnik and S. Akimov, Fiz. Tverd. Tela. **20**, 2815 (1978).
[41] P. Garnier, G. Calvarin, J. F. Berar, and D. Weigel, Mater. Res. Bull. **19**, 407 (1984).
[42] T. Bleser, B. Berge, U. Bismayer, and E. K. H. Salje, J. Phys. Condens. Matter **6**, 2093 (1994).
[43] P. P. Sahoo, E. Gaudin, J. Darriet, and T. N. Guru Row, Inorg. Chem. **49**, 5603 (2010).
[44] O. Aktas, E. K. H. Salje, and M. A. Carpenter, J. Phys. Condens. Matter **25**, 465401 (2013).
[45] H. Yokota, J. Kaneshiro, and Y. Uesu, Phys. Res. Int. **2012**, 1 (2012).
[46] J. Torres, J. Aubree, and J. Brandon, Opt. Commun. **12**, 416 (1974).
[47] U. Bismayer and E. Salje, Acta Crystallogr. Sect. A **37**, 145 (1981).
[48] Y. Yamada and Y. Uesu, Solid State Commun. **81**, 777 (1992).
[49] S. Y. Jeong, M. S. Jang, H. J. Kim, C. R. Cho, and Y. S. Yu, Ferroelectrics **142**, 121 (1993).
[50] B. Wruck, E. K. H. Salje, M. Zhang, T. Abraham, and U. Bismayer, Phase Transitions **48**, 135 (1994).
[51] U. Bismayer, J. Hensler, E. Salje, and B. Güttler, Phase Transitions **48**, 149 (1994).
[52] D. Vanderbilt and R. D. King-Smith, Phys. Rev. B **48**, 4442 (1993).
[53] A. K. Tagantsev and A. S. Yurkov, J. Appl. Phys. **112**, 044103 (2012).
[54] K. Aizu, J. Phys. Soc. Jpn. **28**, 706 (1970).
[55] J. Kaneshiro and Y. Uesu, Phys. Rev. B **82**, 184116 (2010).
[56] J. Sapriel, Phys. Rev. B **12**, 5128 (1975).
[57] I. Tsatskis, D. A. Vul, E. K. H. Salje, and V. Heine, Phase Transitions **52**, 95 (1994).